small methods
www.small-methods.com

Size-Focusing of Au Nanoparticles through Dissolution–Renucleation Process Imaged with In Situ TEM

*Wenhui Wang, Mingyun Zhu, Ivan Erofeev, Guoming Lin, Kuibo Yin, Litao Sun, and Utkur Mirsaidov**

The transformation of large polydisperse nanoparticles (NPs) into small monodisperse ones by adding ligands is an important and powerful post-synthesis method for tuning the size and morphology of NPs. However, the mechanism of this widely used process is not well understood. Here, using in situ liquid-phase transmission electron microscopy (TEM), we show that the steps of this transformation are a complete dissolution of the original NPs and a subsequent renucleation and growth of new, smaller, uniformly-sized NPs. This work offers mechanistic insights into the synthesis of monodisperse NPs and highlights the importance of direct imaging in identifying the physical and chemical details of nanoscale processes that occur in a liquid phase.

1. Introduction

Monodisperse sub-10-nm nanoparticles (NPs) are highly appealing for applications in catalysis,[1–3] energy storage,[4,5] and biomedicine.[6,7] For example, it is well known that the catalytic performance of NPs depends on their size, shape, and composition.[8–10] Hence, to accurately assess how shape or composition affects the activity of NP catalysts, one must use monodisperse NPs as a test system. The common one-step wet chemical synthesis approach[11–14] to produce monodisperse sub-10-nm NPs requires fine-tuning of solvents,[15] ligands,[16–18] additives,[19] and the temperature[20] at which these NPs are synthesized,[21] making the process laborious and time-consuming. Alternatively, monodisperse NPs can be obtained from NPs with an arbitrary size distribution through a post-synthesis process known as digestive ripening.[22,23] The key steps involved in the digestive ripening have been identified as 1) breaking the polydisperse NPs in a colloid into smaller NPs by the addition of ligands, 2) isolating this colloid from the reaction side products, and 3) heating the isolated colloid in the presence of the ligand molecules to form monodisperse NPs.[24] The most interesting chemistry between the NPs and ligands happens in the first step, where small NPs are generated upon the addition of ligands into the polydisperse NPs. The primary role of ligands is to regulate NP shape and size by selectively binding to specific crystal facets, thereby slowing their growth relative to other facets, and to stabilize the NP surface sterically or electrostatically, preventing uncontrolled aggregation and limiting overall size.[16,17,25] However, beyond these intended functions, ligands can also cause unintended effects, such as cracking or dissolving NPs.[22] For example, smaller metallic NPs can be obtained by increasing the ligand-to-metal molar ratio[22] or by increasing the binding energy of the ligand to the metal.[26] Earlier studies attributed the formation of small NPs to ligand-induced cracking of larger NPs at defects and/or with mass transfer from large NPs to smaller ones.[22,26–29] The driving force here is the strong binding of ligands to the NP surface, which significantly decreases the effective surface energy of the NP (and even makes this energy negative).[30] The global minimum of free energy in such a ligand–NP system is thus reached when mass is transferred from bigger particles to the smaller ones, such that all particles become identical in size. This mass transfer process is opposite to the Ostwald ripening process and thus can be used to generate monodisperse colloids. However, this proposed transformation path is deduced only from indirect observation (i.e., by comparing the initial and final NPs)[22,29,31] and lacks validation based on direct evidence. Hence, it remains unclear whether the product NPs evolve from splitting or etching of initial NPs into smaller ones by ligands,[31] or by their partial or complete dissolution, renucleation, and growth into smaller monodisperse NPs.

W. Wang, M. Zhu, G. Lin, U. Mirsaidov
Department of Physics
National University of Singapore
Singapore 117551, Singapore
E-mail: mirsaidov@nus.edu.sg
W. Wang, M. Zhu, I. Erofeev, G. Lin, U. Mirsaidov
Centre for BioImaging Sciences
Department of Biological Sciences
National University of Singapore
Singapore 117557, Singapore
M. Zhu, K. Yin, L. Sun
SEU-FEI Nano-Pico Center
Key Laboratory of MEMS of the Ministry of Education
Southeast University
Nanjing 210096, China
I. Erofeev, U. Mirsaidov
Centre for Advanced 2D Materials and Graphene Research Centre
National University of Singapore
Singapore 117546, Singapore
U. Mirsaidov
Department of Materials Science and Engineering
National University of Singapore
Singapore 117575, Singapore

The ORCID identification number(s) for the author(s) of this article can be found under https://doi.org/10.1002/smtd.202501033

DOI: 10.1002/smtd.202501033

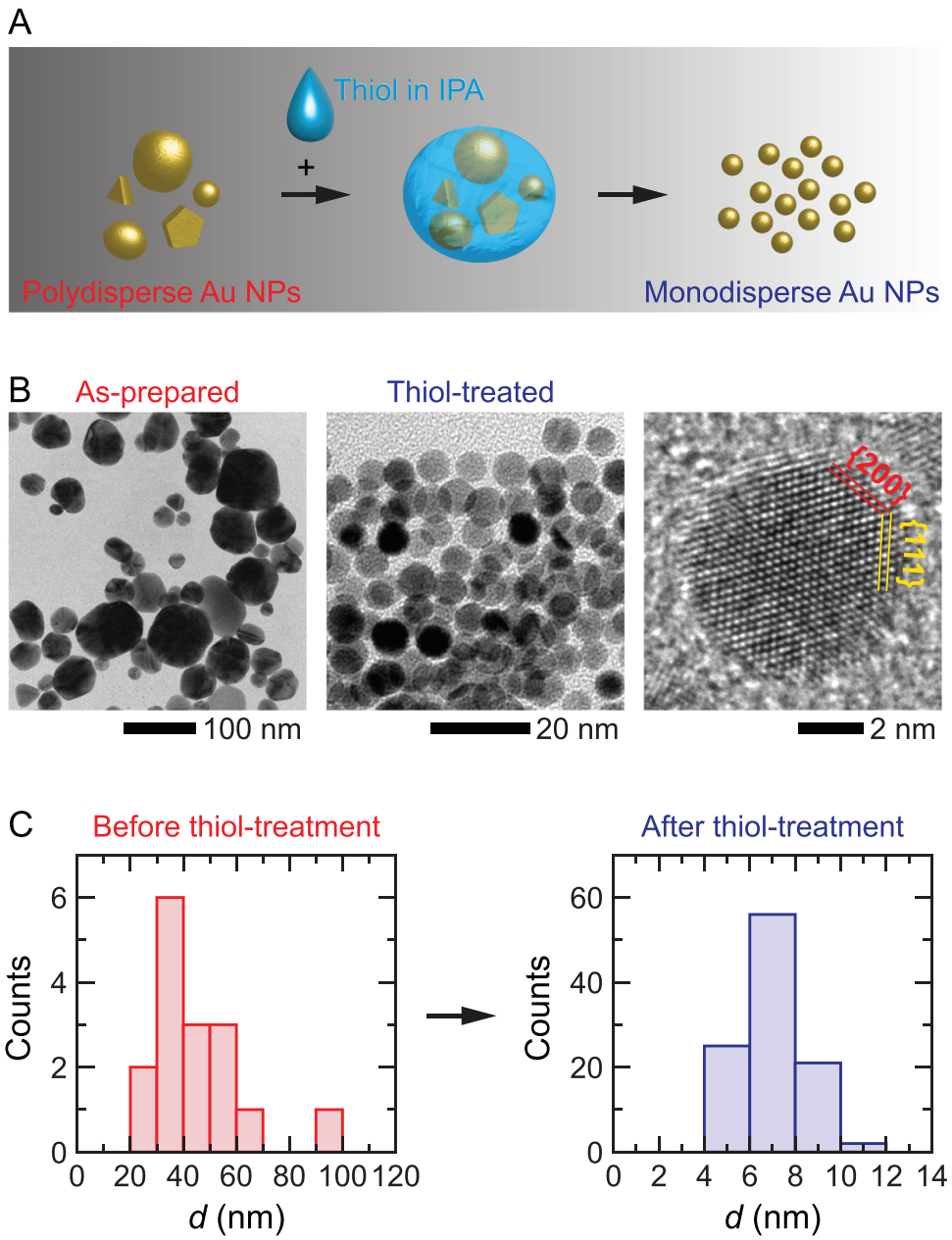

Figure 1. As-prepared and thiol-treated Au NPs. A) Schematic illustration of a transformation of polydisperse Au NPs into small monodisperse Au NPs in an IPA solution of NDT. B) TEM image (*left*) of as-prepared polydisperse Au NPs. Low- and high-magnification TEM images (*middle* and *right*, respectively) of NDT-treated Au NPs. Red and yellow lines mark the spacings of Au {200} and {111} crystal planes, respectively. C) Comparison of Au NP size distributions before and after thiol treatment.

To better understand the NP–ligand interactions, we need to draw a direct connection between the disappearance of large NPs and the appearance of uniform small ones inside the ligand solution. Time-resolved direct imaging in liquids via TEM allows the full sequence of transformations to be tracked, unequivocally connecting the starting NPs to the products.[32–34] Here, using in situ liquid-phase TEM imaging, we investigated how large polydisperse Au NPs evolve into monodisperse NPs in an isopropanol (IPA) solution with 1,9-nonanedithiol (NDT) as ligand. Our results reveal that the transformation is a two-step process, where the initial NPs are first etched by the ligands until they fully dissolve into the solution, followed by nucleation of new NPs from the solution, which grow into monodisperse sub-10-nm NPs.

2. Results and Discussion

Polydisperse Au NPs (**Figure 1B**; Figure S1, Supporting Information) were synthesized via the reverse micelle approach using didodecyldimethylammonium bromide (DDAB) surfactants.[24,28]

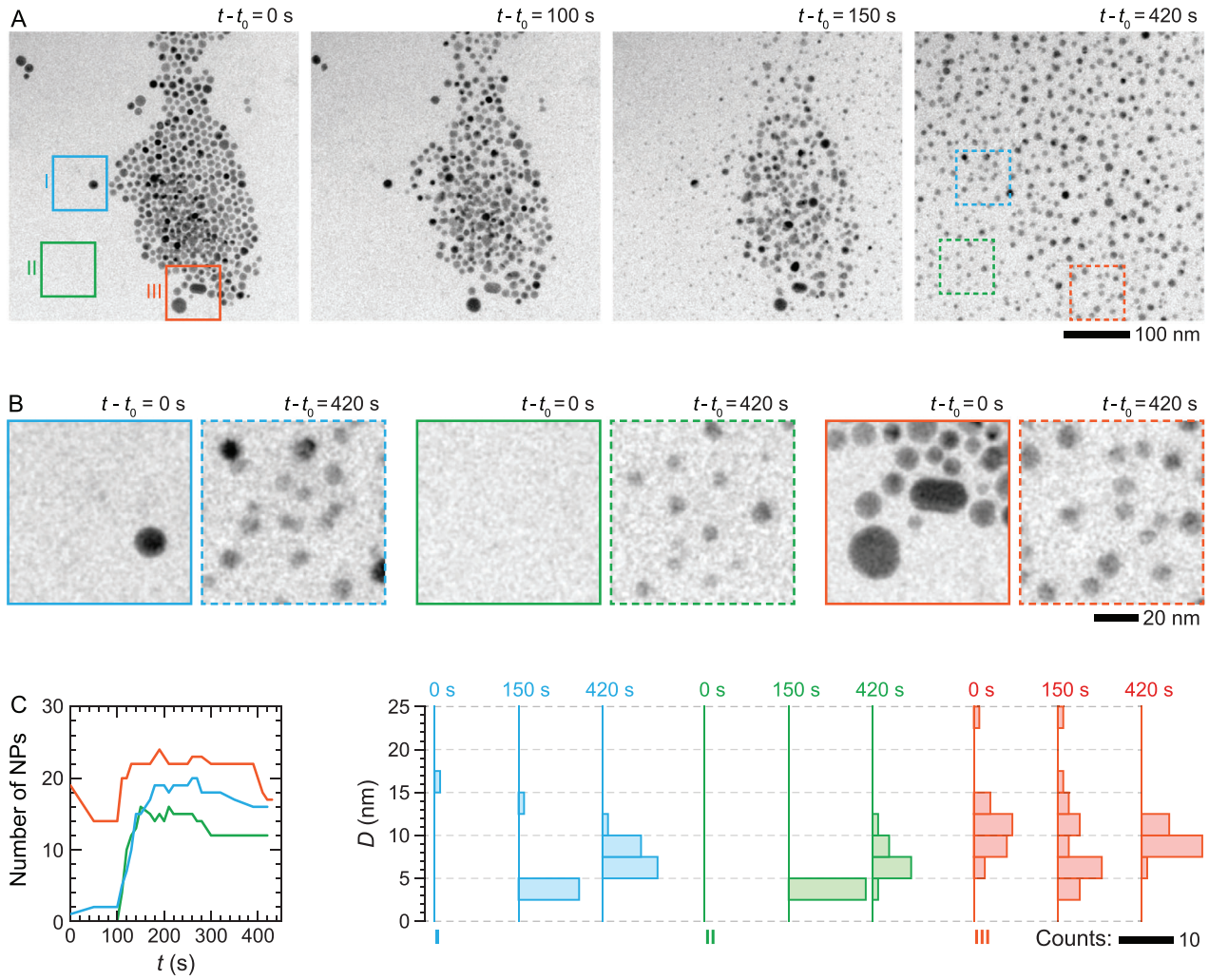

Figure 2. In situ evolution of Au NPs in NDT solution. A) In situ liquid-phase TEM image series showing the evolution of Au NPs in an IPA solution containing NDT (Video S1, Supporting Information). The image series was acquired with an electron flux of $\approx 1\,e^{-}\text{Å}^{-2}\text{s}^{-1}$. B) Enlarged view of Au NPs in the boxed regions shown in (A) (Videos S2–S4, Supporting Information). C) Changes in the number and the size distribution of Au NPs within the boxed regions in (A–B). t_0 corresponds to the time point when the dissolution of the NPs was first noted.

To test the functionality of NDT as a ligand, we treated the as-prepared Au NPs with 60 mM NDT in IPA at room temperature (see the Experimental Section). Note that we used a non-aqueous solvent because thiols are insoluble in water, and we arrived at the optimal ligand concentration of 60 mM through numerous screening tests (Figure S2, Supporting Information). After the NDT treatment, the polydisperse Au NPs transformed into smaller monodisperse spherical Au NPs with a narrow size distribution (Figure 1B,C). To generalize this post-synthesis treatment method, we also explored two other thiol-containing molecules as ligands, and in both cases, the polydisperse Au NPs were converted into sub-10-nm monodisperse Au NPs (Figure S3, Supporting Information). Moreover, we also confirmed that a single NDT treatment step is enough to achieve this monodispersity (e.g., the NPs after four repeated treatments are very similar to those after a single thiol treatment, as shown in Figure S3, Supporting Information).

To understand how polydisperse Au NPs evolve into monodisperse NPs in an NDT solution, we tracked the process using in situ liquid-phase TEM. **Figure 2A** shows that most of the NPs were fully etched and disappeared after introducing the NDT solution into the liquid cell, with smaller-sized NPs disappearing earlier than the larger ones (Figure 2A, $t - t_0 = 0 - 100$ s). As the original NPs dissolve, new NPs start to nucleate everywhere in the solution in a more or less uniform manner across the entire field of view (Figure 2B,C). This nucleation and growth process is consistent with the LaMer model of burst nucleation.[35–37] It is worth mentioning here that even in our control benchtop synthesis experiments, we occasionally find NPs with diameters of less than 3 nm (Figure S4, Supporting Information), which, again, is indicative of nucleation and growth.

Since in situ studies are conducted under an electron beam and on a SiN_x surface, it is important to consider their impact on the observed processes.[38,39] To assess the effect of the beam,

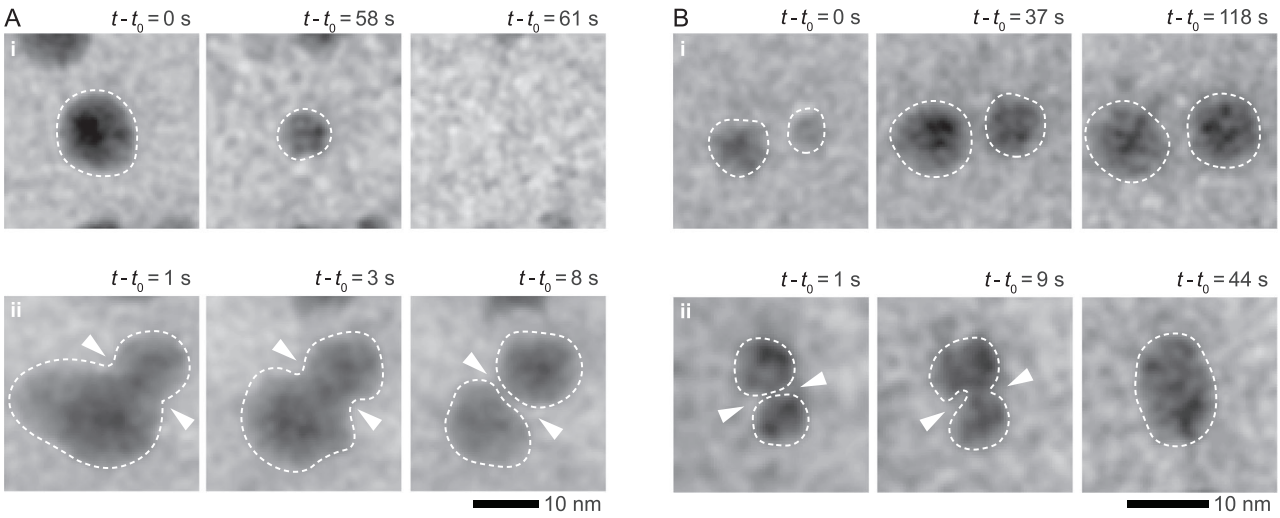

Figure 3. Dissolution and growth of Au NPs in NDT solution. A) In situ liquid-phase TEM image series showing (i) the dissolution and (ii) the splitting (Video S5, Supporting Information) of Au NPs. B) In situ liquid-phase TEM image series showing the growth by (i) monomer attachment and (ii) coalescence (Video S6, Supporting Information) of Au NPs. t_0 corresponds to the time point when the dissolution of the NPs was first noticed. The image series was acquired with an electron flux of $\approx 1 e^{-}\text{Å}^{-2}\text{s}^{-1}$.

we performed multiple control experiments. First, we replaced the NDT (in IPA) solution with pure IPA and imaged the NPs with a similar electron flux. The NPs remained stable under these conditions, with no evident dissolution and nucleation of new NPs (Figure S5, Supporting Information). Second, we compared in situ synthesized NPs under typical imaging conditions with benchtop-synthesized NPs, and for both cases, we found the nanocrystals to have similar size and morphology (Figures 1 vs 2; Figure S6, Supporting Information). Finally, we increased the electron flux to probe its effect on the final NPs morphology and found that for a typical electron flux of 1 e^{-} Å^{-2} s^{-1} or less used throughout our study, the in situ synthesized NPs were similar to the benchtop-synthesized ones (Figures S7 and S8, Supporting Information). To exclude the effect of substrates (i.e., carbon film of a TEM grid or SiN_x film of a liquid cell) on which our size-focusing studies were performed on the dissolution and nucleation of NPs in the NDT solution, we compared the NPs obtained from the same reaction conditions but on different substrates. Figure S9 (Supporting Information) shows that polydisperse Au NPs transformed into monodisperse NPs when the reaction was carried out i) inside a solution, ii) on an FDTS-treated hydrophobic substrate, and iii) on an APTES-treated hydrophilic substrate, as those seen on a carbon film or bare SiN_x film (Figures 1B and 2A vs Figure S9, Supporting Information). Hence, we conclude that the substrate has no significant effect on the observed transformation of polydisperse NPs into sub-10-nm NPs.

We took a detailed look at how individual NPs transform during the reaction. The initial dissolution of large NPs occurs mainly through two pathways, as shown in **Figure** 3A: i) direct dissolution and ii) the splitting of big NPs into smaller ones, followed by dissolution (Figure S10, Supporting Information). Growth also occurs through two pathways, as shown in Figure 3B: i) growth by monomer addition and ii) coalescence. It is worth noting that while the coalescence of NPs at different stages of their growth can produce NPs with varying sizes,[40,41] it is a rare event, and only <1% of the final NPs here are formed through coalescence.

Based on the presented data, the NP dissolution, nucleation, and growth can be understood as follows. The original solution contains Au NPs capped with DDAB surfactant molecules. Thiol-containing ligands have a much stronger affinity to Au than DDAB, so when NDT is added to the solution, the NP surface undergoes ligand exchange. Due to the strong S—Au bonding, the adsorption of thiols on the surface of the Au NP weakens the bond between the surface Au atoms and their nearest neighbors (Figure S11, Supporting Information).[42] When a thiol ligand detaches from the surface of the NP, it removes one Au atom. Over time, thiols etch the original NPs, saturating the solution with Au atoms. As Au atoms rapidly diffuse and spread uniformly in the solution, saturation occurs everywhere simultaneously, leading to the rapid nucleation and growth of NPs everywhere. As Au atoms in the solution are depleted, growth stops everywhere simultaneously, producing NPs of similar size that are stabilized by NDT ligands in the solution, preventing their aggregation (Figure 2C).

While the dissolution–renucleation process produces uniform NPs, there is another process that may impact the size distribution of these NPs. At later stages of the growth, as the density of smaller NPs increases, some NPs may grow at the expense of others through Ostwald ripening. This, in turn, may broaden the size distribution as some NPs get larger, as shown in **Figure** 4.[43,44] While this is not a significant issue because we found that only ≈5% undergo the Oswald ripening, our direct observation provides insight into how to further improve the monodispersity of the NP. Since Ostwald ripening happens at a later stage of the growth, after the uniformity has already been achieved (Figure 4B: $t - t_0 = 205 - 421$ s), one can envision quenching the reaction earlier, before the onset of the Ostwald ripening.

Another factor to consider is the impact of temperature on size-focusing, as temperature affects the rate of ligand

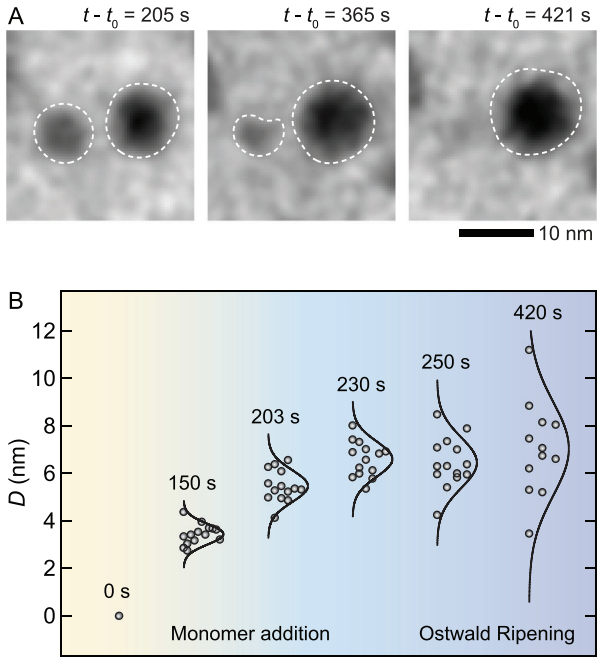

Figure 4. Ostwald ripening of Au NPs in NDT solution. A) In situ liquid-phase TEM image series showing the Ostwald ripening of two adjacent Au NPs from region II, displayed in Figure 2. B) Diameter of NPs (in region II shown in Figure 2) as a function of time, showing the broadening of their size distribution caused by Ostwald ripening at the later stages of the growth ($t - t_0 \geq 250$ s). The curves are the Gaussian fits to the distribution. The image series was acquired with an electron flux of $\approx 1 e^{-} \text{Å}^{-2} \text{s}^{-1}$.

exchange.[22,45] To investigate the effect of temperature on the growth process, morphology, and size distribution of the NPs, we first introduced the as-prepared Au NPs into an 80 °C NDT solution and examined the products of the reaction. **Figure 5A** shows that the reaction at 80 °C also produces monodisperse spherical Au NPs, similar to those formed at room temperature. However, in this case, we found that the NPs tend to cluster together. Interestingly, NPs in the clusters possess aligned lattice orientations, as suggested by the selected area electron diffraction image in Figure 5A. Note that this clustering is not caused by capillary forces during drying of the NPs on a TEM grid because a similar clustering process can also be seen in solution in in situ liquid-phase TEM image series (Figure 5B). These image series reveal that initially, several NPs nucleate and grow closely to each other without coalescing (Figure 5B, $t - t_0 = 18$ s) until they reach a stable size of ≈8 nm (Figure 5B, $t - t_0 = 44$ s). While it is beyond the scope of this study, it is worth noting that the growth of NPs in assembled clusters during rapid growth at higher temperatures is not unusual and often attributed to balanced attractive and repulsive interparticle interactions between ligand-capped NP.[46]

3. Conclusion

In conclusion, by directly following the size-focusing of Au NPs with liquid-phase TEM, we identified the steps involved in this process. These steps are: 1) the dissolution of initial polydisperse NPs induced by the thiol functional groups of ligands, followed by 2) the subsequent nucleation and growth of new, smaller monodisperse NPs. These observations contrast with earlier indirect studies that attribute size-focusing of NPs to etching and splitting processes. Hence, our study provides valuable insights needed to synthesize uniform NPs for a wide range of applications.

4. Experimental Section

Materials: Following reagents were used in this study: Gold(III) chloride trihydrate ($HAuCl_4 \cdot 3H_2O$, Cat. No. 520918, Sigma–Aldrich Co., St Louis, MO, USA), sodium borohydride ($NaBH_4$, Cat. No. 452882, Sigma–Aldrich Co., St Louis, MO, USA), 1,9-nonanedithiol (NDT, Cat No. N29805, Sigma–Aldrich Co., St Louis, MO, USA), didodecyldimethylammonium bromide (DDAB, Cat No. 359025, Sigma–Aldrich Co., St Louis, MO, USA), 1H,1H,2H,2H-perfluorodecyltrichlorosilane (FDTS, Cat. No. AB111155, abcr GmbH, Karlsruhe, Germany), 3-aminopropyltriethoxysilane (APTES, Cat. No. AB110815, abcr GmbH, Karlsruhe, Germany), isopropanol (IPA, Cat, No. VWRC20882.320, VWR Singapore Pte Ltd, Singapore), and toluene (Cat No. 179418, Sigma–Aldrich Co., St Louis, MO, USA).

Polydisperse Au NPs Synthesis: Polydisperse Au NPs were synthesized using a slightly modified reverse micelle method described by Prasad et al.[47,48] Specifically, 20 mg of $HAuCl_4 \cdot 3H_2O$ was dissolved in 5 mL of 15 mM DDAB toluene solution and ultrasonicated for 5 min. Then, 60 µL of 4 M freshly prepared $NaBH_4$ aqueous solution was added to this mixed solution dropwise while stirring mildly with a magnetic stir bar. After stirring the reaction solution for 15 min, Au ions are reduced completely, forming NPs, and the color of the solution turns dark purple.

Thiol Treatment on As-Prepared Polydisperse NPs: A simple post-treatment approach was adopted for the as-prepared NPs. First, 3 µL of as-prepared polydisperse Au NPs dispersion was drop-cast onto a copper grid with carbon film. The grid was dried under ambient conditions for 5 min. Then, 5 µL of 60 mM NDT in IPA solution was drop-cast onto the grid. The grid was again left to dry under an ambient condition. The drop-casting of the thiol solution was repeated at four different time points, following the same procedure as described above for studies shown in Figure 1B and Figure S3 (Supporting Information). For thiol treatment at elevated temperature, after drop-casting the thiol solution, the grid was dried at 80 °C for 10 min in an oven.

In Situ Liquid-Phase TEM Experiments: For room-temperature in situ liquid-phase TEM studies, liquid cells comprising two custom-fabricated chips with a 25-nm-thick SiN_x window were used.[49] Approximately 500 nL of as-prepared Au dispersion was drop-cast onto the bottom chip and allowed to dry at ambient conditions. The top and bottom chips were assembled together and sealed within a liquid flow holder (Hummingbird Scientific, Lacey, WA, USA) after their SiN_x film windows were aligned. After checking and confirming that there were no leaks in the flow cell, the entire assembly was loaded into a TEM for in situ imaging. A 60 mM NDT in IPA solution was introduced into the cell through fluid tubing (with a diameter of 200 µm and length of ≈50 cm) at a flow rate of 2 µL min^{-1} using a syringe pump, and the reaction was imaged in real time. After the start of the flow, it usually took a couple of minutes for the liquid to reach the window area of the liquid cell and come into contact with the Au NPs.

For in situ heating studies, liquid cells comprising one custom-fabricated top chip and one heating bottom chip were used. The heating chips were calibrated using the software and parameters provided by Hummingbird Scientific, and the temperature was calculated based on the resistivity of the heating element. The temperature fluctuation during the experiment was ≈±10 °C. Heating was initiated along with the flow of the thiol solution.

Imaging and Image Processing: For the study, two TEMs were used. High-resolution TEM (HRTEM) and STEM images were acquired using a 300 kV Titan TEM (Thermo Fisher Scientific, Hillsboro, OR, USA) and a Gatan K2 IS CMOS camera (Gatan Inc., Pleasanton, CA, USA). The in situ liquid-phase TEM studies were performed using a 200 kV JEOL

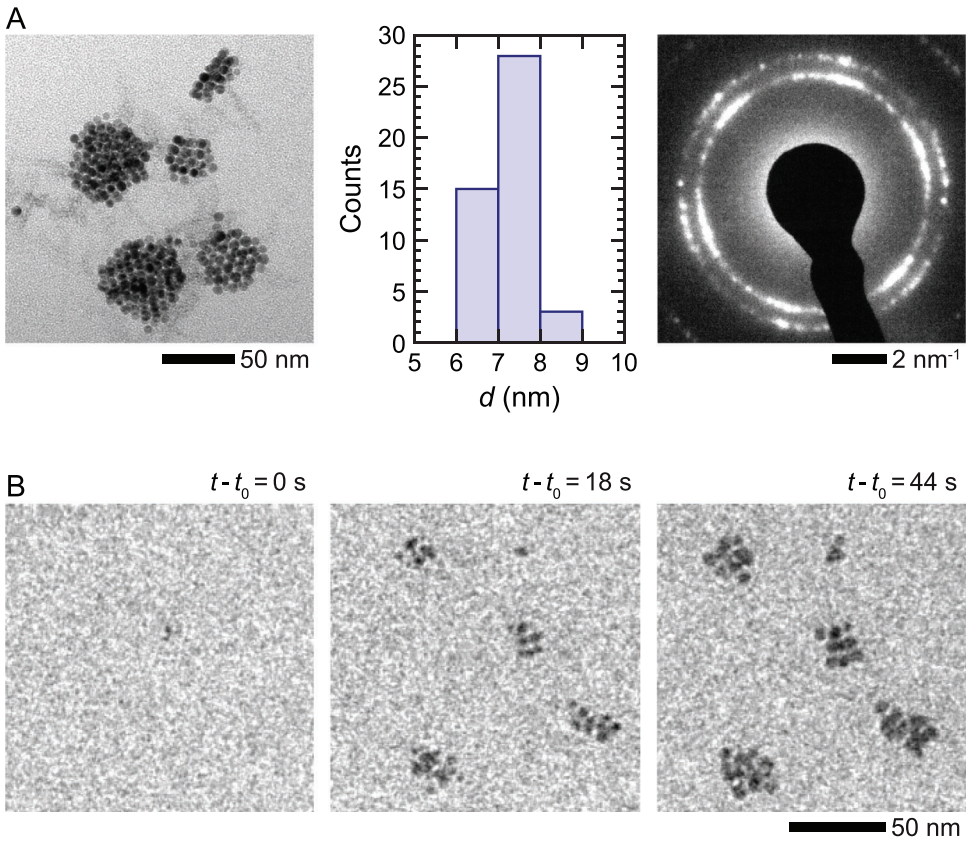

Figure 5. Au NPs ensembles formed in NDT solution at 80 °C. A) TEM image of benchtop-synthesized Au NP clusters after 60 mM NDT solution treatment at 80 °C, size distribution of product NPs, and selected area electron diffraction of one NP cluster. B) In situ TEM image series of the growth stage of the digestive ripening process, which displays the nucleation and growth of monodisperse NPs into clusters in 60 mM NDT (in IPA) solution at 80 °C (Video S7, Supporting Information). The image series was acquired with an electron flux of $\approx 1 e^{-}\text{Å}^{-2}\text{s}^{-1}$.

2010F TEM (JEOL Ltd., Tokyo, Japan) equipped with a Gatan OneView camera (Gatan Inc., Pleasanton, CA, USA). The in situ image series was acquired at a rate of 5 frames per second, using an incident electron flux of $< 1 e^{-}\text{Å}^{-2}\text{s}^{-1}$.

All image processing algorithms for the analysis of in situ image series files were written in Python 3.7[50] using Numpy,[51] Scipy,[50] OpenCV,[52] HyperSpy,[53] and matplotlib[54] libraries. The raw dm4 format files (Gatan Inc., Pleasanton, CA, USA) were converted into 8-bit.png images. The images were first scaled down by a factor of 2, and then the image sequence was drift corrected using cross-correlation template matching,[55] followed by averaging over 2–10 frames, depending on the contrast of the images, to improve the signal-to-noise ratio. After these preprocessing steps, the boundaries of selected NPs were manually segmented.

Statistical Analysis: The number of NPs and their corresponding sizes, displayed in histograms in Figures 1C, 2C, and 4B, were manually counted and measured.

Supporting Information

Supporting Information is available from the Wiley Online Library or from the author.

Acknowledgements

This work was supported by the Singapore Ministry of Education's Academic Research Fund Tier 2 (MOE-MOET2EP10120-0004). M.Z. acknowledges the support of the China Scholarship Council (202106090065).

Conflict of Interest

The authors declare no conflict of interest.

Data Availability Statement

The data that support the findings of this study are available in the supplementary material of this article.

Keywords

digestive ripening, in situ TEM, nanoparticles, size-focusing, synthesis

Received: June 3, 2025
Revised: September 7, 2025
Published online: October 22, 2025

[1] A. S. K. Hashmi, *Science* **2012**, *338*, 1434.
[2] L. Liu, M. Lopez-Haro, C. W. Lopes, C. Li, P. Concepcion, L. Simonelli, J. J. Calvino, A. Corma, *Nat. Mater.* **2019**, *18*, 866.
[3] X. Huang, O. Akdim, M. Douthwaite, K. Wang, L. Zhao, R. J. Lewis, S. Pattisson, I. T. Daniel, P. J. Miedziak, G. Shaw, D. J. Morgan, S. M. Althahban, T. E. Davies, Q. He, F. Wang, J. Fu, D. Bethell, S. McIntosh, C. J. Kiely, G. J. Hutchings, *Nature* **2022**, *603*, 271.

[4] Y. Lu, W. Chen, *Chem. Soc. Rev.* **2012**, *41*, 3594.
[5] P. Zhang, X. Zhao, Z. Liu, F. Wang, Y. Huang, H. Li, Y. Li, J. Wang, Z. Su, G. Wei, Y. Zhu, L. Fu, Y. Wu, W. Huang, *NPG Asia Mater.* **2018**, *10*, 429.
[6] H. Xiang, W. Feng, Y. Chen, *Adv. Mater.* **2020**, *32*, 1905994.
[7] Q. Liu, Y. Sun, T. Yang, W. Feng, C. Li, F. Li, *J. Am. Chem. Soc.* **2011**, *133*, 17122.
[8] Y. Yang, S. Louisia, S. Yu, J. Jin, I. Roh, C. Chen, M. V. Fonseca Guzman, J. Feijóo, P.-C. Chen, H. Wang, C. J. Pollock, X. Huang, Y.-T. Shao, C. Wang, D. A. Muller, H. D. Abruña, P. Yang, *Nature* **2023**, *614*, 262.
[9] S. Cao, F. Tao, Y. Tang, Y. Li, J. Yu, *Chem. Soc. Rev.* **2016**, *45*, 4747.
[10] E. D. Goodman, S. Dai, A.-C. Yang, C. J. Wrasman, A. Gallo, S. R. Bare, A. S. Hoffman, T. F. Jaramillo, G. W. Graham, X. Pan, M. Cargnello, *ACS Catal.* **2017**, *7*, 4372.
[11] N. T. K. Thanh, N. Maclean, S. Mahiddine, *Chem. Rev.* **2014**, *114*, 7610.
[12] K.-J. Wu, E. C. M. Tse, C. Shang, Z. Guo, *Prog. Mater. Sci.* **2022**, *123*, 100821.
[13] N. Mac Fhionnlaoich, S. Guldin, *Chem. Mater.* **2020**, *32*, 3701.
[14] M. L. Personick, C. A. Mirkin, *J. Am. Chem. Soc.* **2013**, *135*, 18238.
[15] W. Niu, Y. Duan, Z. Qing, H. Huang, X. Lu, *J. Am. Chem. Soc.* **2017**, *139*, 5817.
[16] A. Heuer-Jungemann, N. Feliu, I. Bakaimi, M. Hamaly, A. Alkilany, I. Chakraborty, A. Masood, M. F. Casula, A. Kostopoulou, E. Oh, K. Susumu, M. H. Stewart, I. L. Medintz, E. Stratakis, W. J. Parak, A. G. Kanaras, *Chem. Rev.* **2019**, *119*, 4819.
[17] J.-M. Nam, J. S. Owen, D. V. Talapin, *Acc. Chem. Res.* **2023**, *56*, 2265.
[18] F. M. Schenk, S. Wintersteller, J. Clarysse, H. He, J.-M. von Mentlen, N. Yazdani, M. Wied, V. Wood, C. Prehal, M. Yarema, *J. Am. Chem. Soc.* **2025**, *147*, 12105.
[19] H.-E. Lee, H.-Y. Ahn, J. Mun, Y. Y. Lee, M. Kim, N. H. Cho, K. Chang, W. S. Kim, J. Rho, K. T. Nam, *Nature* **2018**, *556*, 360.
[20] J. Li, Y. Li, Q. Li, Z. Wang, F. Leonard Deepak, *Nanoscale Horiz.* **2019**, *4*, 1302.
[21] G. Gnanaprakash, S. Mahadevan, T. Jayakumar, P. Kalyanasundaram, J. Philip, B. Raj, *Mater. Chem. Phys.* **2007**, *103*, 168.
[22] J. R. Shimpi, D. S. Sidhaye, B. L. V. Prasad, *Langmuir* **2017**, *33*, 9491.
[23] D. S. Sidhaye, B. L. V. Prasad, *New J. Chem.* **2011**, *35*, 755.
[24] B. L. V. Prasad, S. I. Stoeva, C. M. Sorensen, K. J. Klabunde, *Chem. Mater.* **2003**, *15*, 935.
[25] J. Li, F. L. Deepak, *Chem. Rev.* **2022**, *122*, 16911.
[26] P. Sahu, B. L. Prasad, *Nanoscale* **2013**, *5*, 1768.
[27] S. P. Bhaskar, M. Vijayan, B. R. Jagirdar, *J. Phys. Chem. C* **2014**, *118*, 18214.
[28] S. I. Stoeva, V. Zaikovski, B. L. V. Prasad, P. K. Stoimenov, C. M. Sorensen, K. J. Klabunde, *Langmuir* **2005**, *21*, 10280.
[29] B. L. V. Prasad, S. I. Stoeva, C. M. Sorensen, K. J. Klabunde, *Langmuir* **2002**, *18*, 7515.
[30] V. M. Burlakov, A. Goriely, *Appl. Sci.* **2020**, *10*, 5359.
[31] X. Chen, M. Wei, S. Jiang, S. Förster, *Langmuir* **2019**, *35*, 12130.
[32] F. M. Ross, *Science* **2015**, *350*, aaa9886.
[33] U. Mirsaidov, J. P. Patterson, H. Zheng, *MRS Bull.* **2020**, *45*, 704.
[34] R. Yang, L. Mei, Y. Fan, Q. Zhang, H.-G. Liao, J. Yang, J. Li, Z. Zeng, *Nat. Protoc.* **2023**, *18*, 555.
[35] C. B. Whitehead, S. Özkar, R. G. Finke, *Chem. Mater.* **2019**, *31*, 7116.
[36] D. B. K. Chu, J. S. Owen, B. Peters, *J. Phys. Chem. A* **2017**, *121*, 7511.
[37] A. Baronov, K. Bufkin, D. W. Shaw, B. L. Johnson, D. L. Patrick, *Phys. Chem. Chem. Phys.* **2015**, *17*, 20846.
[38] T. J. Woehl, T. Moser, J. E. Evans, F. M. Ross, *MRS Bull.* **2020**, *45*, 746.
[39] N. M. Schneider, M. M. Norton, B. J. Mendel, J. M. Grogan, F. M. Ross, H. H. Bau, *J. Phys. Chem. C* **2014**, *118*, 22373.
[40] F. Wang, V. N. Richards, S. P. Shields, W. E. Buhro, *Chem. Mater.* **2014**, *26*, 5.
[41] H. Wang, M. Mutailipu, L. Boddapati, A. Samanta, F. L. Deepak, J. Li, *J. Am. Chem. Soc.* **2025**, *147*, 22104.
[42] J. R. Reimers, M. J. Ford, A. Halder, J. Ulstrup, N. S. Hush, *Proc. Natl. Acad. Sci. USA* **2016**, *113*, E1424.
[43] W. Dachraoui, T. R. Henninen, D. Keller, R. Erni, *Sci. Rep.* **2021**, *11*, 23965.
[44] N. L. Visser, S. J. Turner, J. A. Stewart, B. D. Vandegehuchte, J. E. S. van der Hoeven, P. E. de Jongh, *ACS Nano* **2023**, *17*, 14963.
[45] P. Sahu, B. L. Prasad, *Langmuir* **2014**, *30*, 10143.
[46] L. Wu, J. J. Willis, I. S. McKay, B. T. Diroll, J. Qin, M. Cargnello, C. J. Tassone, *Nature* **2017**, *548*, 197.
[47] X. M. Lin, H. M. Jaeger, C. M. Sorensen, K. J. Klabunde, *J. Phys. Chem. B* **2001**, *105*, 3353.
[48] X. M. Lin, G. M. Wang, C. M. Sorensen, K. J. Klabunde, *J. Phys. Chem. B* **1999**, *103*, 5488.
[49] Q. Liu, F. Y. Leong, Z. Aabdin, U. Anand, T. S. B. Quang, U. Mirsaidov, *ACS Nano* **2015**, *9*, 9020.
[50] T. E. Oliphant, *Comput. Sci. Eng.* **2007**, *9*, 10.
[51] S. v. d. Walt, S. C. Colbert, G. Varoquaux, *Comput. Sci. Eng.* **2011**, *13*, 22.
[52] G. Bradski, *Dr. Dobb's J. Softw. Tools Prof. Program.* **2000**, *25*, 120.
[53] F. De La Peña, T. Ostasevicius, V. T. Fauske, P. Burdet, P. Jokubauskas, M. Nord, E. Prestat, M. Sarahan, K. E. MacArthur, D. N. Johnstone, J. Taillon, J. Caron, T. Furnival, A. Eljarrat, S. Mazzucco, V. Migunov, T. Aarholt, M. Walls, F. Winkler, B. Martineau, G. Donval, E. R. Hoglund, I. Alxneit, I. Hjorth, L. F. Zagonel, A. Garmannslund, C. Gohlke, I. Iyengar, H.-W. Chang, *hyperspy/hyperspy: HyperSpy 1.3*, Zenodo, Geneva, Switzerland **2017**.
[54] J. D. Hunter, *Comput. Sci. Eng.* **2007**, *9*, 90.
[55] R. C. Gonzalez, R. E. Woods, *Digital Image Processing*, Pearson, New York **2018**.